



Superdiffusion of quantized vortices uncovering scaling laws in quantum turbulence

Yuan Tang^{a,b}, Shiran Bao^{a,b}, and Wei Guo^{a,b,1}

^aThe Cryogenics Laboratory, National High Magnetic Field Laboratory, Tallahassee, FL 32310; and ^bMechanical Engineering Department, Florida State University, Tallahassee, FL 32310

Edited by Vanderlei S. Bagnato, University of Sao Paulo, Sao Carlos, Brazil, and approved January 4, 2021 (received for review October 20, 2020)

Generic scaling laws, such as Kolmogorov's 5/3 law, are milestone achievements of turbulence research in classical fluids. For quantum fluids such as atomic Bose–Einstein condensates, superfluid helium, and superfluid neutron stars, turbulence can also exist in the presence of a chaotic tangle of evolving quantized vortex lines. However, due to the lack of suitable experimental tools to directly probe the vortex-tangle motion, so far little is known about possible scaling laws that characterize the velocity correlations and trajectory statistics of the vortices in quantum-fluid turbulence, i.e., quantum turbulence (QT). Acquiring such knowledge could greatly benefit the development of advanced statistical models of QT. Here we report an experiment where a tangle of vortices in superfluid ⁴He are decorated with solidified deuterium tracer particles. Under experimental conditions where these tracers follow the motion of the vortices, we observed an apparent superdiffusion of the vortices. Our analysis shows that this superdiffusion is not due to Lévy flights, i.e., long-distance hops that are known to be responsible for superdiffusion of random walkers. Instead, a previously unknown power-law scaling of the vortex–velocity temporal correlation is uncovered as the cause. This finding may motivate future research on hidden scaling laws in QT.

quantum turbulence | superfluid | superdiffusion | particle tracking velocimetry | scaling laws

Quantum fluids, such as superfluids, superconductors, and Bose–Einstein condensates (BECs), exhibit macroscopic quantum coherence that is responsible for their dissipationless motion (1). In these quantum fluids, all rotational motion is sustained by quantized vortex lines, i.e., line-shaped topological defects characterized by a circulating flow of particles with a discrete circulation $\kappa = h/m$, where h is Planck's constant and m is the mass of the particle.

Turbulence in quantum fluids, i.e., quantum turbulence (QT), can be induced by a tangle of interacting vortex lines (2). These vortex lines evolve chaotically under their self-induced and mutually induced velocities and can reconnect when they move across each other (3). The underlying science of QT is broadly applicable to a variety of coherent physical systems, such as coherent condensed-matter systems [e.g., superfluid ³He and ⁴He (4), atomic and polariton BECs (5), and type II superconductors (6)], cosmic systems [e.g., neutron-pair superfluid in neutron stars (7, 8), cosmic strings in the Abelian–Higgs model (9), and possible axion dark matter BECs in galactic halos (10)], and even complex light fields (11). Insight into the generic scaling laws that characterize the evolution of quantized vortex tangles can inform statistical models of QT, which could have a broad significance spanning multiple branches of physics.

QT research has been conducted mostly in superfluid ³He and ⁴He due to the material's accessibility and the wide range of length scales involved in their turbulence behaviors (12). Nevertheless, despite extensive theoretical and numerical studies of the vortex-line dynamics in superfluid helium (13–15), past experimental research has largely been limited to the measurements

of spatially averaged quantities such as the vortex-line density L (i.e., length of vortices per unit volume) (16–18) or local pressure and temperature variations (19, 20). Important statistical properties of a fully developed vortex tangle, such as the vortex–velocity correlations and their trajectory statistics, remain largely unexplored due to the lack of experimental tools for probing the vortex-line motion.

A breakthrough has been made in recent years with the development of quantitative flow visualization techniques (21). In particular, by decorating the vortices in superfluid ⁴He (He II) with solidified hydrogen particles, Bewley et al. (22) demonstrated direct vortex-line visualization. Since then, vortex-line reconnections and Kelvin-wave excitations on individual vortices have been filmed (23–25). Nevertheless, visualization data showing the real-time evolution of a complex vortex tangle are still lacking, which impedes the development of reliable statistical models for describing QT (26).

In our recent experiment on He II QT driven by an applied heat current, we seeded the fluid with solidified deuterium (^D₂) tracer particles and observed that a group of particles could remain trapped on the tangled vortices (27–30). By applying a separation scheme in data analysis (28), we were able to track solely these trapped particles and therefore could directly probe the vortex-tangle dynamics. In this paper, we discuss our study of the apparent diffusion of these trapped particles under experimental conditions where they faithfully follow the motion of the evolving vortices.

We report the observation of a superdiffusion of the vortices in the tangle when their root-mean-square displacement (rmsd) is less than the mean intervortex distance $\ell = L^{-1/2}$. Surprisingly, our analysis shows that this superdiffusion is not due

Significance

Quantum turbulence (QT) can appear in the presence of a chaotic tangle of quantized vortices in various quantum-fluid systems, including atomic Bose–Einstein condensates, superfluid helium, superfluid neutron stars, etc. Insights into the generic scaling behaviors of tangled vortices are crucial in developing an advanced statistical model of QT. By tracking tracer particles trapped on vortices in superfluid ⁴He, we report the observation of an apparent superdiffusion of the vortices in QT. Our analysis shows that this superdiffusion is not due to Lévy flights, i.e., long-distance hops that are responsible for superdiffusion of random walkers. Instead, a power-law scaling of the vortex–velocity correlation is identified as the cause. This finding may motivate extensive future research on hidden scaling laws in QT.

Author contributions: W.G. designed research; Y.T. performed research; Y.T., S.B., and W.G. analyzed data; and Y.T., S.B., and W.G. wrote the paper.

The authors declare no competing interest.

This article is a PNAS Direct Submission.

Published under the PNAS license.

¹To whom correspondence may be addressed. Email: wguo@magnet.fsu.edu.

Published February 1, 2021.

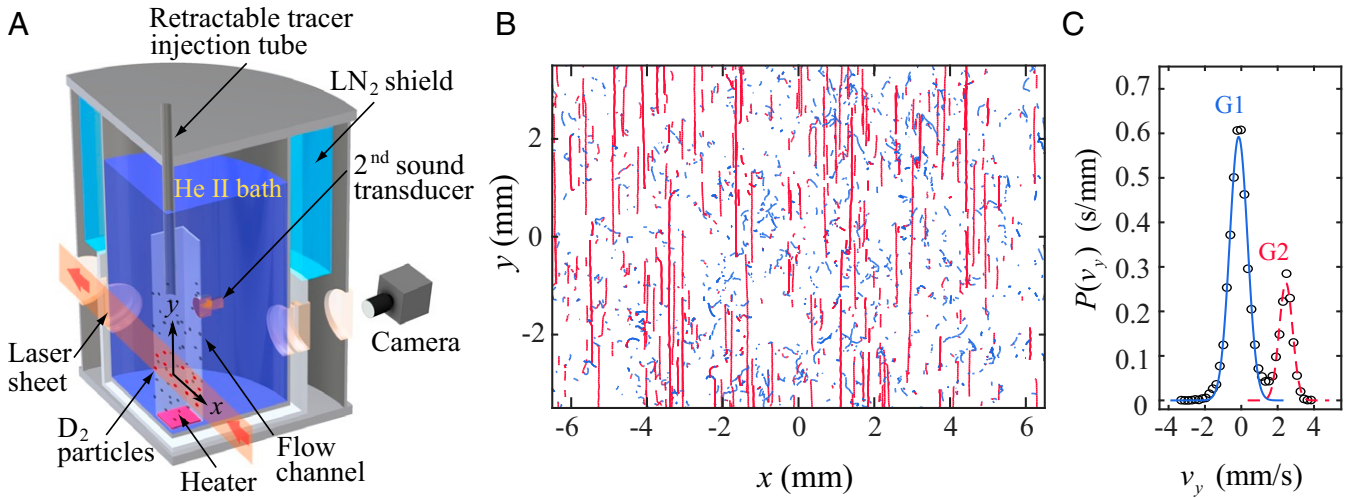


Fig. 1. (A) A schematic diagram of the experimental setup. (B) Representative trajectories obtained at $T = 1.85$ K and $q = 38$ mW/cm² in He II for G1 particles trapped on vortices (blue) and G2 particles entrained by the normal fluid (red). (C) The corresponding streamwise particle-velocity distribution, where the solid and the dashed curves represent Gaussian fits to the data.

to Lévy flights (i.e., randomized, long-distance hops) that are known to be responsible for superdiffusion in various physical and nonphysical systems (31). Instead, we reveal that a previously unknown power-law scaling of the vortex-velocity temporal correlation is the cause. The derived power-law exponent appears to be temperature and vortex-line density independent, suggesting that the observed scaling behaviors may be generic properties of a fully developed random vortex tangle. These findings may excite future research on hidden scaling laws in QT.

Results

Experimental Setup and Procedures. Our experimental setup is shown schematically in Fig. 1A. A 400- Ω planar resistive heater is installed at the bottom of a vertical flow channel ($1.6 \times 1.6 \times 33$ cm³) inside a He II bath. The temperature T of the He II in the bath can be controlled by regulating the vapor pressure. When a direct current voltage is applied to the heater, a counterflow of the two interpenetrating fluid components of He II establishes in the flow channel (32): The viscous normal-fluid component that consists of thermal quasiparticles in He II (i.e., phonons and rotons) flows away from the heater at a mean velocity given by $v_n = q/\rho s T$, where q is the heat flux, and ρ and s are the He II density and specific entropy, respectively; while the inviscid superfluid component (i.e., the condensate) moves in the opposite direction at a velocity $v_s = -v_n \rho_n / \rho_s$, where ρ_n / ρ_s is the density ratio of the two fluids.

It has been known that above a small threshold heat flux of the order 10 mW/cm² (33), turbulence appears spontaneously in the superfluid as a random tangle of quantized vortex lines, each carrying a quantized circulation $\kappa \simeq 10^{-3}$ cm²/s around its angstrom-sized core (3). A mutual friction between the two fluids arises due to scattering of the thermal quasiparticles off the vortices (34). Above a heat flux of the order 10² mW/cm², the normal fluid can also become turbulent (35–37), rendering a complex doubly turbulent system (38–41). Our current research focuses on the low heat flux regime where only the superfluid is turbulent.

To probe the flow, we adopt a particle-tracking velocimetry (PTV) technique using solidified D₂ particles as tracers. Due to their small sizes (i.e., about 4 μ m in diameter) (42), these particles have a small Stokes number in the normal fluid and hence are entrained by the viscous normal-fluid flow (43). But when they are close to the vortex cores, a Bernoulli pressure due to the superfluid flow induced by the vortex cores can push the particles

toward the cores (3), resulting in the trapping of the particles on the quantized vortex lines. These tracer particles are illuminated by a thin continuous-wave laser sheet and their positions are recorded by a video camera at 90 Hz. We have also installed a pair of second-sound transducers for measuring the vortex-line density using a standard second-sound attenuation method (44). More details can be found in *Materials and Methods*.

As we reported in refs. 28–30, two distinct groups of particles can be observed at q below about 10² W/cm² (Fig. 1B). The G1 group includes particles entrapped on vortices, resulting in irregular trajectories. The G2 group includes untrapped particles entrained by the up-moving laminar normal fluid, resulting in relatively straight trajectories. The streamwise particle velocity distribution based on the analysis of all trajectories exhibits two nearly separated peaks (Fig. 1C), which allows us to distinguish these two groups of particles for separately analyzing their motion (28). The mean velocity of the G2 particles equals the expected normal-fluid velocity. The G1 particles are carried by the vortex tangle which drifts at v_s toward the heater at small q (45), but in general the G1 particles may also slide along the vortices due to the viscous drag from the normal fluid.

Nevertheless, at q less than a few tens of mW/cm², we find that the mean velocity of the G1 particles is about v_s (28), in

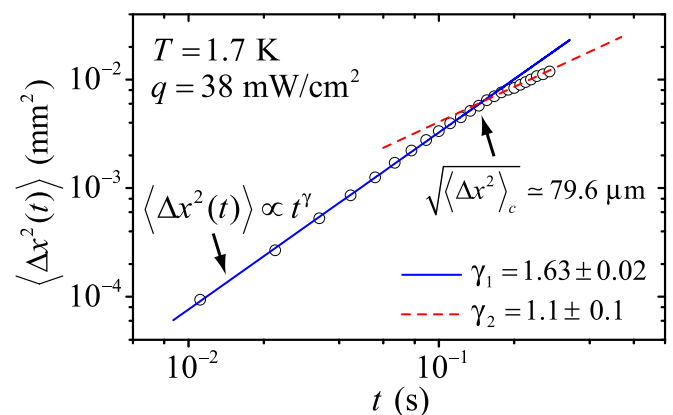


Fig. 2. Representative data showing the horizontal mean-square displacement $\langle \Delta x^2(t) \rangle$ of the G1 particles as a function of the diffusion time t . The solid and the dashed lines are power-law fits to the data.

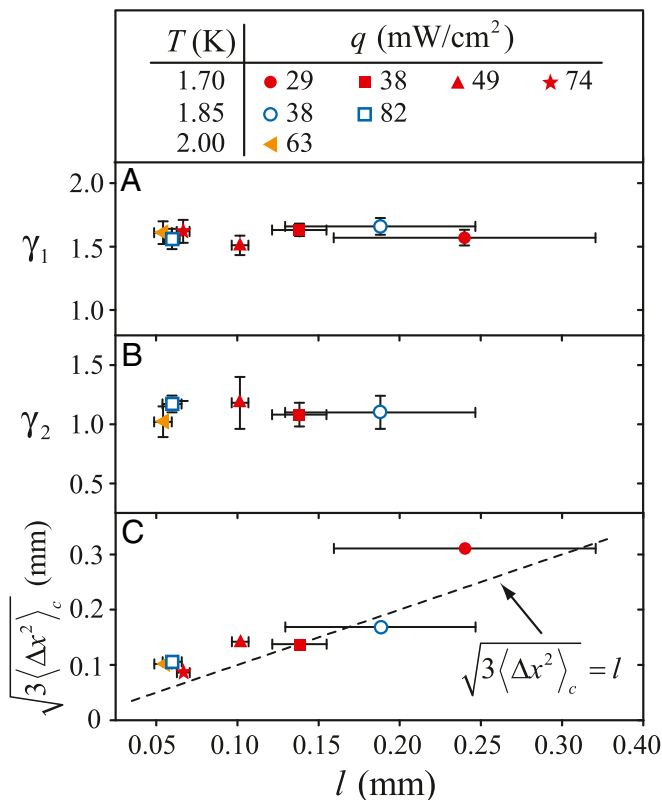


Fig. 3. A and B show, respectively, the obtained scaling exponents γ_1 and γ_2 for the two diffusion regimes of the G1 particles. (C) A comparison of the transition rmsd with the mean intervortex distance ℓ . The vertical error bars represent the uncertainties in the power-law fits as shown in Fig. 2, and the horizontal error bars denote the standard deviation of the measured ℓ . At small vortex-line density L (i.e., large ℓ), the increased measurement uncertainty leads to large horizontal error bars.

agreement with the observations of Paoletti et al. (46, 47). This observation suggests that the viscous drag effect on the trapped G1 particles should be mild in the low heat-flux regime. Furthermore, a recent theoretical work suggests that micrometer-sized tracers trapped on quantized vortex lines in He II are indeed immobilized along the lines due to an effective friction originating from the breakdown of the vortex coherence (48). Therefore, in the low heat flux regime, it is feasible to explore the genuine vortex-tangle dynamics by tracking the motion of the trapped G1 particles. Specifically, we focus on studying the apparent diffusion of the G1 particles in the horizontal direction to keep the viscous drag influence minimal.

Vortex Diffusion Statistics. For the data obtained at each temperature and heat flux, we first calculate the horizontal mean-square displacement of the G1 particles $\langle \Delta x^2(t) \rangle = \langle [x(t) - x(0)]^2 \rangle$, where the diffusion time t starts from the moment when a particle is first observed along its trajectory, and the angle brackets denote an ensemble average over at least 10^3 trajectories. In general, a power-law scaling $\langle \Delta x^2(t) \rangle \propto t^\gamma$ is expected, where the exponent γ is often used to identify different types of diffusions, i.e., normal diffusion ($\gamma = 1$), superdiffusion ($\gamma > 1$), and subdiffusion ($\gamma < 1$) (49). Fig. 2 shows a representative result obtained at $T = 1.7$ K and $q = 38$ W/cm². The data exhibit two power-law scaling regimes: a superdiffusion regime with $\gamma_1 \approx 1.63$ at small rmsd (i.e., $\sqrt{\langle \Delta x^2 \rangle}$) and a nearly normal diffusion regime with $\gamma_2 \approx 1.1$ at larger rmsd. These two regimes intersect at $\sqrt{\langle \Delta x^2 \rangle_c} \approx 79.6$ μm . Due to their irregular tra-

jectories, the G1 particles seldom stay in the thin laser plane for a long time. Therefore, we have relatively few long trajectories to study the G1 particle diffusion at large t , which limits the range of the observed γ_2 -scaling regime. We also comment that at sufficiently small diffusion times, the vortex segments are expected to move ballistically at the local superfluid velocity (3), which should lead to a t^2 scaling of $\langle \Delta x^2 \rangle$. However, this distinct regime likely would occur only below a few milliseconds for the vortex-line density examined in our experiments, which is beyond the resolution of typical He II PTV measurements.

Our analysis of the datasets obtained at other heat fluxes and temperatures also shows similar two-power-law scaling regimes. The derived γ_1 , γ_2 , and $\sqrt{\langle \Delta x^2 \rangle_c}$ are collected in Fig. 3. Surprisingly, in the explored temperature range of 1.7 to 2.0 K where ρ_n/ρ_s varies from 0.3 to 1.24 (50), the γ_1 value is always around 1.6 to 1.7 while γ_2 is close to unity, regardless of the applied heat fluxes. This suggests that the observed diffusion scalings could be generic properties of an evolving random vortex tangle. We have also examined the transition rmsd that separates the two diffusion regimes and find that $\sqrt{\langle \Delta x^2 \rangle_c}$ increases with decreasing the vortex-line density L . Considering the fact that the diffusion occurs in three-dimensional (3D) space, we compare $\sqrt{3\langle \Delta x^2 \rangle_c}$ with the measured intervortex distance ℓ in Fig. 3C. These two quantities agree reasonably, suggesting that the transition occurs when the rmsd of the vortices is greater than ℓ .

It is worthwhile noting that the spatial spreading of a decaying isolated vortex tangle at $T = 0$ K either near a solid surface (51) or in bulk He II (52) has been simulated. The growth of the tangle diameter d as reported in ref. 52 exhibits a normal diffusion regime at large t and a clear superdiffusion regime at small t with a fitted scaling of about $d^2 \propto t^{1.74}$ (note that the authors interpreted this latter regime as the ballistic regime). This similarity is encouraging, although our work focuses on the trajectory statistics of vortices in a steady tangle at finite temperatures.

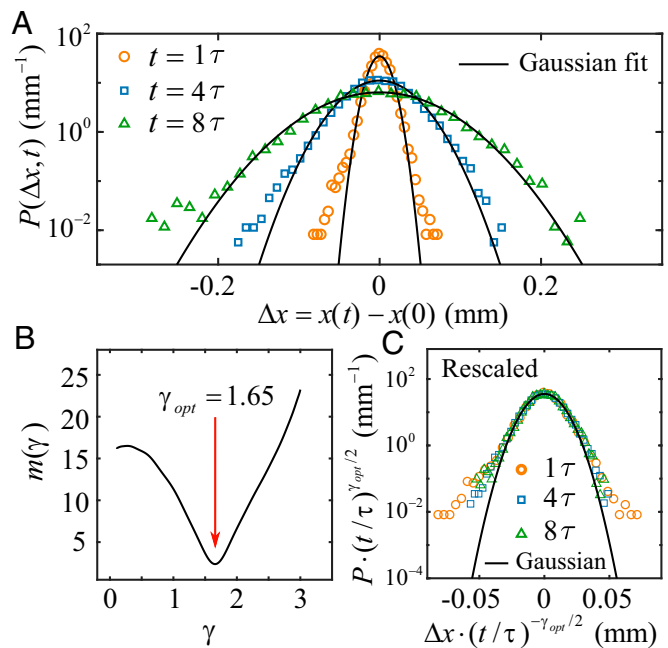


Fig. 4. (A) Representative particle-displacement distribution function $P(\Delta x, t)$ for the data obtained at 1.7 K and 29 mW/cm². (B) The measure of the self-similarity m versus the scaling exponent γ . (C) The rescaled profiles of $P(\Delta x, t)$.

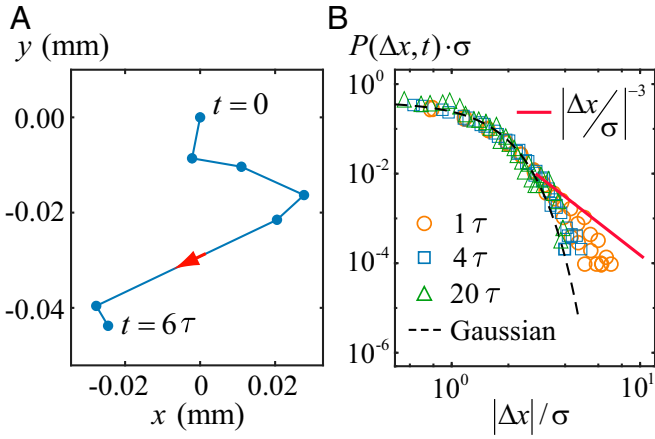


Fig. 5. (A) An example G1 particle trajectory that exhibits one large step displacement. (B) The tail profiles of $P(\Delta x, t)$, normalized by the standard deviation σ of Δx , at different t . The data were taken at 1.7 K and 29 mW/cm².

Furthermore, following ref. 52, we can use our data in the normal diffusion regime to evaluate the effective diffusion coefficient $\nu'/\kappa = 3\langle\Delta x^2(t)\rangle/4t$. For the data shown in our Fig. 2, we get $\nu'/\kappa \simeq 0.3$, which is close to the simulated values (51, 52).

Vortex-Displacement Distribution. Naturally, one would wonder about the cause of the observed vortex-line superdiffusion and why there is a transition to normal diffusion at $\sqrt{3\langle\Delta x^2\rangle_c} \sim \ell$. Indeed, superdiffusion has been observed in a wide range of systems, such as the motion of cold atoms in an optical lattice (53), the chaotic drifting of tracers in rotating flows (54), the cellular transport in biological systems (55), and even the search patterns of human hunter-gatherers (56). A useful function for characterizing superdiffusion is the distribution function $P(\Delta x, t)$ of the particle displacement Δx at time t , whose time evolution is often described by a fractional diffusion equation (57). A general property of $P(\Delta x, t)$ is the existence of a self-similar scaling $P(\Delta x, t) = (t/t')^{-\frac{\gamma}{2}} \cdot P(\Delta x \cdot (t/t')^{-\frac{\gamma}{2}}, t')$, where the scaling exponent γ should be identical to the diffusion exponent of the mean-square displacement (31). To test whether this property holds for the apparent diffusion of the G1 particles, we examine the $P(\Delta x, t)$ profiles at different t for the data taken at 1.7 K and 29 mW/cm² (see example profiles in Fig. 4A). We use the profile at $t = \tau$ as the reference, where $\tau \simeq 11$ ms is the time step set by the camera frame rate. To determine the optimal exponent γ_{opt} that gives the best match among the $P(\Delta x, t)$ profiles after the rescaling, we minimize the profile difference by calculating the standard L_1 -type variance (53)

$$m(\gamma) = \sum_{t=\tau}^{N\tau} \frac{\int | (t/\tau)^{\frac{\gamma}{2}} \cdot P(\Delta x \cdot (t/\tau)^{-\frac{\gamma}{2}}, t) - P(\Delta x, \tau) | dx}{\int P(\Delta x, \tau) dx}, \quad [1]$$

where the summation goes over all of the $P(\Delta x, t)$ profiles obtained at $t \in [\tau, N\tau]$, where $N\tau$ is the maximum diffusion time in the γ_1 -scaling regime. Fig. 4B shows the calculated variance m as a function of γ . The minimum m is achieved at $\gamma_{opt} = 1.65$, which is indeed close to the diffusion scaling exponent $\gamma_1 = 1.57$ for the chosen dataset. As shown in Fig. 4C, the rescaled $P(\Delta x, t)$ profiles overlap very well except perhaps in the tail region.

Indeed, for superdiffusion systems involving random walkers, another important property of $P(\Delta x, t)$ is its non-Gaussian tails. It has been identified that superdiffusion in those systems is caused by long-distance hops of the walkers (53–57), i.e.,

the so-called Lévy flights (31). These flights lead to asymptotic power-law tails of the step-displacement distribution $P(\Delta x, \tau) \propto |\Delta x|^{-\alpha}$ with $\alpha < 3$ (58). After many steps, the resulting $P(\Delta x, t)$ converges to a Lévy distribution with similar power-law tails. The variance $\langle\Delta x^2\rangle$ for such a heavy-tailed distribution diverges, but a pseudovariance behavior $\langle\Delta x^2(t)\rangle \propto t^\gamma$ with $\gamma = \frac{2}{\alpha-1}$ can be derived through a scaling argument (31, 57, 58), resulting in an apparent superdiffusion (i.e., $\gamma > 1$ when $\alpha < 3$). Without such fat tails (i.e., if $\alpha \geq 3$), $\langle\Delta x^2\rangle$ would converge, which then leads to a Gaussian distribution of $P(\Delta x, t)$ and hence a normal diffusion of the walkers according to the central limit theorem (58).

Interestingly, the trapped G1 particles do exhibit occasional long-distance hops over the time step τ . An example G1 trajectory that contains an exceptionally large step displacement is shown in Fig. 5A. The origin of these long-distance hops has been understood as due to the particles carried by vortex segments that are close to locations of vortex reconnections (29). As revealed by Paoletti et al. (46), vortex reconnections result in local high vortex-velocity occurrences, which lead to non-Gaussian $|v|^{-3}$ tails of the vortex-line velocity distribution. Therefore, when τ is small, the step-displacement distribution of the vortex lines should acquire similar power-law tails $P(\Delta x, \tau) \propto |\Delta x|^{-3}$. However, since the velocities of the reconnecting vortex segments become high only within a short time window centered at the moment of reconnections, over longer time t the total displacement of a vortex segment $\Delta x = \int_0^t v_x(t') dt'$ would rarely exhibit exceptionally large values. Therefore, the tails of the resulting $P(\Delta x, t)$ are suppressed. To see this effect, we show the tails of $P(\Delta x, t)$ at different t in Fig. 5B for the data taken at 1.7 K and 29 mW/cm². Obviously, as t increases from τ to 20τ , the tail changes from close to $|\Delta x|^{-3}$ to nearly a Gaussian form. This observation is similar in nature to what was reported in ref. 59. Therefore, despite the existence of some long-distance hops of the G1 particles at small time steps, their statistical weight is not sufficient to render the observed superdiffusion.

Vortex-Velocity Correlation. Without invoking Lévy flights, superdiffusion may still emerge if the motion of the particles is not completely random but instead exhibits extended temporal correlations (58, 60). For quantized vortices in a vortex tangle, the chaotic motion of the vortex segments is driven by their self-induced and mutually induced velocities (3). There is no

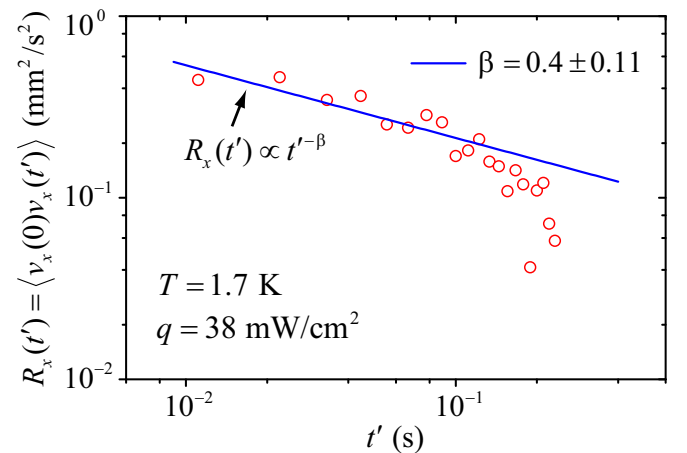


Fig. 6. The calculated horizontal-velocity temporal correlation function $R_x(t')$ for the data taken at 1.7 K and 38 mW/cm². The solid line represents a power-law fit.

existing knowledge on whether this motion is completely random or indeed has a certain temporal correlation.

Mathematically, the mean-square displacement $\langle \Delta x^2(t) \rangle$ of a vortex-line segment can be evaluated based on its velocity $v_x(t)$ as (61)

$$\langle \Delta x^2(t) \rangle = 2 \int_0^t dt_0 \int_0^{t-t_0} dt' \langle v_x(t_0) v_x(t_0 + t') \rangle, \quad [2]$$

where the horizontal-velocity temporal correlation function $R_x(t', t_0) = \langle v_x(t_0) v_x(t_0 + t') \rangle$ for statistically steady and homogeneous systems would depend only on the lapse time t' ; i.e., $R_x(t') = \langle v_x(0) v_x(t') \rangle$. In this situation, if a power-law scaling $R_x(t') \propto (t')^{-\beta}$ exists, one can easily derive from Eq. 2 that the mean-square displacement will scale as $\langle \Delta x^2(t) \rangle \propto t^{2-\beta}$. On the other hand, if $R_x(t')$ drops rapidly with t' , a normal diffusion can be obtained. In Fig. 6, we show the calculated $R_x(t')$ for the representative dataset included in Fig. 2. At small lapse time t' , the data do exhibit a power-law scaling with β of about 0.4. This scaling exponent leads to $\langle \Delta x^2(t) \rangle \propto t^{1.6}$, which agrees nicely with the observed superdiffusion. Furthermore, $R_x(t')$ drops sharply beyond a transition time that coincides with the transition to the normal diffusion as seen in Fig. 2, which naturally explains this transition. Similar $R_x(t')$ scaling behaviors are also observed for other datasets. These observations provide direct evidence showing the existence of a possible generic power-law scaling of the vortex-velocity temporal correlation at scales less than ℓ for a random vortex tangle.

Discussion

The analyses that we have presented support the following simple physical picture. The trapped G1 particles move with the quantized vortices in the tangle whose velocities exhibit a power-law temporal correlation. This correlation leads to an apparent superdiffusion of the vortex lines in 3D space. But when their rmsd becomes greater than the mean intervortex distance ℓ , the vortices are expected to move across each other and hence would undergo reconnections. Following the reconnections, the resulting vortex lines move apart toward directions that are distinct from their original directions (23, 25), a process that effectively randomizes the motion of the vortices. This randomization then leads to a sharp drop of the vortex-velocity temporal correlation and hence results in the normal diffusion of the vortices at large length and time scales.

Note that the spatial velocity correlation functions of vortices in atomic condensates have been simulated (62, 63), where the authors reported a rapid decay of the correlation over a length scale comparable to ℓ . But to test the physical picture we have outlined, numerical simulations similar to ref. 64 need to be conducted so that the temporal correlation of the vortex velocity in steady counterflow turbulence can be examined. Indeed, our communication with the authors of ref. 64 has returned encouraging news that their recent simulation does reproduce the power-law scaling of the vortex-velocity correlation as depicted in Fig. 6. These authors also notice that the derived diffusion exponent γ_1 is nearly temperature independent, thereby supporting our observation about the generic nature of this diffusion scaling.

In summary, our work demonstrates that examining the velocity correlations and trajectory statistics of individual vortices in a vortex tangle could uncover hidden scaling properties of QT. Along the lines, many intriguing questions may be raised. For instance, what is the mechanism underlying the observed power-law scaling of the vortex-velocity temporal correlation for a random tangle? Does this scaling also hold for a vortex tangle with large-scale polarizations? How do superfluid parcels

Table 1. Measured vortex-line density L

T (K)	q (mW/cm ²)	L (cm ⁻²)
1.70	74	$(22.5 \pm 1.0) \times 10^3$
	49	$(9.7 \pm 1.0) \times 10^3$
	38	$(5.5 \pm 1.3) \times 10^3$
	29	$(1.7 \pm 1.1) \times 10^3$
1.85	82	$(28.2 \pm 3.2) \times 10^3$
	38	$(2.8 \pm 1.7) \times 10^3$
2.00	63	$(34.9 \pm 6.1) \times 10^3$

undergo apparent diffusion and dispersion in QT? We hope that these questions will stimulate more future research on vortex and superfluid dynamics.

Materials and Methods

Particle-Tracking Velocimetry. We use solidified deuterium (D_2) particles as tracers in He II. These tracer particles are produced by slowly injecting a mixture of 5% D_2 gas and 95% ^4He gas directly into the He II bath via a gas injection system similar to what Fonda et al. (65) reported. Upon the injection, the D_2 gas forms small ice particles with a mean diameter of about 4 μm , as determined from their settling velocity in quiescent He II (42). Following the particle injection, we then turn on the heater and wait for 10 to 20 s for a steady counterflow to establish in the flow channel. A continuous-wave laser sheet (thickness, 200 μm ; height, 9 mm) passes through the geometric center of the channel to illuminate the particles. The positions of the particles in the illuminated plane are captured by a video camera at 90 frames per second. At a given temperature and heat flux, we took a sequence of 720 images and would typically repeat this data acquisition three times to obtain enough particle trajectories for statistical analyses. A modified feature-point tracking routine (66) is adopted to extract the trajectories of the tracer particles from the sequence of images. The velocity of a particle can be determined by dividing its displacement from one frame to the next by the frame separation time.

Separation Data Analysis Scheme. To determine whether a tracer particle belongs to the G1 group (i.e., particles that are trapped on vortices) or the G2 group (i.e., untrapped particles that are entrained by the normal fluid), a separation data analysis scheme is adopted (28). As shown in Fig. 1C, the vertical-velocity distribution based on the analysis of all particle trajectories exhibits two nearly separated peaks at low heat fluxes. Through Gaussian fits to these two peaks, we can determine their respective mean velocities (i.e., \bar{v}_1 and \bar{v}_2) and the corresponding standard deviations (i.e., σ_1 and σ_2). Then, for a particle with a vertical velocity $v_y < \bar{v}_2 - a_2\sigma_2$, it is categorized as a G1 particle. Otherwise, if $v_y > \bar{v}_1 + a_1\sigma_1$, the particle is treated as a G2 particle. Depending on how far the G1 and the G2 peaks are separated, the coefficients a_1 and a_2 are adjusted in the range of 2 to 6 to better distinguish the two groups. Most of the particle trajectories can be identified as either the G1 type or the G2 type. At relatively large heat fluxes, some trajectories may appear to be partly the G1 type and partly the G2 type. This is due to the particles originally moving with the normal fluid later getting trapped by vortex lines (i.e., G2 to G1) or the trapped particles getting released during vortex reconnections (i.e., G1 to G2). In the current work, we focus on analyzing the whole and partial trajectories that are identified as the G1 type.

Second-Sound Attention. We measure the volume-averaged vortex-line density L in the flow channel using the standard second-sound attenuation method (44). Due to its two-fluid nature, He II supports two distinct sound modes: an ordinary pressure-density wave (i.e., the first sound), where both fluids move in phase, and a temperature-entropy wave (i.e., the second sound), where the two fluids move out of phase. The second-sound waves can be generated and picked up by oscillating superleak transducers (44). These transducers are essentially parallel plate capacitors with one fixed plate and one flexible plate made of a thin porous membrane coated with an evaporated gold layer. By applying an alternating current to one transducer as shown in Fig. 1A, a standing second-sound wave across the channel width can be established, whose amplitude can be measured by the other transducer installed on the opposite channel wall. In the presence of quantized vortices, the amplitude of the second-sound wave is attenuated, and

the degree of this attenuation can be used to calculate the vortex-line density L (42). Table 1 lists our measurement results under various temperatures and heat fluxes.

Data Availability. All study data related to this work, including the flow visualization videos, have been deposited in Open Science Framework (10.17605/OSF.IO/YQUZV).

1. D. Tilley, J. Tilley, *Superfluidity and Superconductivity* (Taylor & Francis, 1990).
2. W. F. Vinen, J. J. Niemela, Quantum turbulence. *J. Low Temp. Phys.* **128**, 167–231 (2002).
3. R. J. Donnelly, *Quantized Vortices in Helium II* (Cambridge University Press, 1991), vol. 2.
4. C. F. Barenghi, R. J. Donnelly, W. F. Vinen, *Quantized Vortex Dynamics and Superfluid Turbulence* (Springer, Berlin, Germany, 2001).
5. L. Madeira, M. A. Caracanhas, F. E. A. dos Santos, V. S. Bagnato, Quantum turbulence in quantum gases. *Annu. Rev. Condens. Matter Phys.* **11**, 37–56 (2020).
6. D. Larbalestier, A. Gurevich, D. M. Feldmann, A. Polyanskii, High- T_c superconducting materials for electric power applications. *Nature* **414**, 368–377 (2001).
7. G. Greenstein, Superfluid turbulence in neutron stars. *Nature* **227**, 791–794 (1970).
8. N. Andersson, T. Sidery, G. L. Comer, Superfluid neutron star turbulence. *Mon. Not. R. Astron. Soc.* **381**, 747–756 (2007).
9. W. H. Zurek, Cosmological experiments in superfluid-helium. *Nature* **317**, 505–508 (1985).
10. P. Sikivie, Q. Yang, Bose-Einstein condensation of dark matter axions. *Phys. Rev. Lett.* **103**, 111301 (2009).
11. S. N. Alperin, A. L. Grotelueschen, M. E. Siemens, Quantum turbulent structure in light. *Phys. Rev. Lett.* **122**, 044301 (2019).
12. C. F. Barenghi, L. Skrbek, K. R. Sreenivasan, Introduction to quantum turbulence. *Proc. Natl. Acad. Sci. U.S.A.* **111**, 4647–4652 (2014).
13. K. W. Schwarz, Three-dimensional vortex dynamics in superfluid ^4He : Homogeneous superfluid turbulence. *Phys. Rev. B* **38**, 2398–2417 (1988).
14. H. Adachi, S. Fujiyama, M. Tsubota, Steady-state counterflow quantum turbulence: Simulation of vortex filaments using the full Biot-Savart law. *Phys. Rev. B* **81**, 104511 (2010).
15. A. W. Baggaley, J. Laurie, C. F. Barenghi, Vortex-density fluctuations, energy spectra, and vortical regions in superfluid turbulence. *Phys. Rev. Lett.* **109**, 205304 (2012).
16. S. R. Stalp, L. Skrbek, R. J. Donnelly, Decay of grid turbulence in a finite channel. *Phys. Rev. Lett.* **82**, 4831–4834 (1999).
17. V. B. Eltsov *et al.*, Quantum turbulence in a propagating superfluid vortex front. *Phys. Rev. Lett.* **99**, 265301 (2007).
18. P. Walmsley, D. Zmeev, F. Pakpour, A. Golov, Dynamics of quantum turbulence of different spectra. *Proc. Natl. Acad. Sci. U.S.A.* **111** (suppl. 1), 4691–4698 (2014).
19. J. Maurer, P. Tabeling, Local investigation of superfluid turbulence. *Europhys. Lett.* **43**, 29–34 (1998).
20. D. I. Bradley *et al.*, Direct measurement of the energy dissipated by quantum turbulence. *Nat. Phys.* **7**, 473–476 (2011).
21. W. Guo, M. La Mantia, D. P. Lathrop, S. W. Van Sciver, Visualization of two-fluid flows of superfluid helium-4. *Proc. Natl. Acad. Sci. U.S.A.* **111** (suppl. 1), 4653–4658 (2014).
22. G. P. Bewley, D. P. Lathrop, K. R. Sreenivasan, Superfluid helium: Visualization of quantized vortices. *Nature* **441**, 588 (2006).
23. G. P. Bewley, M. S. Paoletti, K. R. Sreenivasan, D. P. Lathrop, Characterization of reconnecting vortices in superfluid helium. *Proc. Natl. Acad. Sci. U.S.A.* **105**, 13707–13710 (2008).
24. E. Fonda, D. P. Meichle, N. T. Ouellette, S. Hormoz, D. P. Lathrop, Direct observation of kelvin waves excited by quantized vortex reconnection. *Proc. Natl. Acad. Sci. U.S.A.* **111** (suppl. 1), 4707–4710 (2014).
25. E. Fonda, K. R. Sreenivasan, D. P. Lathrop, Reconnection scaling in quantum fluids. *Proc. Natl. Acad. Sci. U.S.A.* **116**, 1924–1928 (2019).
26. S. K. Nemirovskii, Quantum turbulence: Theoretical and numerical problems. *Phys. Rep.* **524**, 85–202 (2013).
27. B. Mastracci, S. Takada, W. Guo, Study of particle motion in He II counterflow across a wide heat flux range. *J. Low Temp. Phys.* **187**, 446 (2017).
28. B. Mastracci, W. Guo, Exploration of thermal counterflow in He II using particle tracking velocimetry. *Phys. Rev. Fluids* **3**, 063304 (2018).
29. B. Mastracci, W. Guo, Characterizing vortex tangle properties in steady-state He II counterflow using particle tracking velocimetry. *Phys. Rev. Fluids* **4**, 023301 (2019).
30. B. Mastracci, S. Bao, W. Guo, W. F. Vinen, Particle tracking velocimetry applied to thermal counterflow in superfluid ^4He : Motion of the normal fluid at small heat fluxes. *Phys. Rev. Fluids* **4**, 083305 (2019).
31. V. Zaburdaev, S. Denisov, J. Klafter, Lévy walks. *Rev. Mod. Phys.* **87**, 483–530 (2015).
32. L. D. Landau, E. M. Lifshitz, *Fluid Mechanics* (Pergamon Press, Oxford, UK, ed. 2, 1987), vol. 6.
33. W. F. Vinen, Mutual friction in a heat current in liquid helium II. IV. Critical heat currents in wide channels. *Proc. R. Soc. A* **243**, 400–413 (1958).
34. W. F. Vinen, Mutual friction in a heat current in liquid helium II. III. Theory of the mutual friction. *Proc. R. Soc. A* **242**, 493–515 (1957).
35. A. Marakov *et al.*, Visualization of the normal-fluid turbulence in counterflowing superfluid ^4He . *Phys. Rev. B* **91**, 094503 (2015).

ACKNOWLEDGMENTS. We acknowledge the valuable discussions with W. F. Vinen and D. Kivotides. We also thank S. Yui, H. Kobayashi, and M. Tsubota for communicating their recent simulation results. This work is supported by the NSF under Grant DMR-1807291 and the US Department of Energy under Grant DE-SC0020113. The experiment was conducted at the National High Magnetic Field Laboratory at Florida State University, which is supported through the NSF Cooperative Agreement DMR-1644779 and the state of Florida.

36. J. Gao, W. Guo, W. F. Vinen, Determination of the effective kinematic viscosity for the decay of quasiclassical turbulence in superfluid ^4He . *Phys. Rev. B* **94**, 094502 (2016).
37. J. Gao, E. Varga, W. Guo, W. F. Vinen, Energy spectrum of thermal counterflow turbulence in superfluid helium-4. *Phys. Rev. B* **96**, 094511 (2017).
38. J. Gao *et al.*, Decay of counterflow turbulence in superfluid ^4He . *JETP Lett.* **103**, 648–652 (2016).
39. J. Gao, E. Varga, W. Guo, W. F. Vinen, Statistical measurement of counterflow turbulence in superfluid helium-4 using He_2^+ tracer-line tracking technique. *J. Low Temp. Phys.* **187**, 490 (2017).
40. J. Gao, W. Guo, S. Yui, M. Tsubota, W. F. Vinen, Dissipation in quantum turbulence in superfluid ^4He above 1 K. *Phys. Rev. B* **97**, 184518 (2018).
41. S. Bao, W. Guo, V. S. L'vov, A. Pomyalov, Statistics of turbulence and intermittency enhancement in superfluid ^4He counterflow. *Phys. Rev. B* **98**, 174509 (2018).
42. B. Mastracci, W. Guo, An apparatus for generation and quantitative measurement of homogeneous isotropic turbulence in He II. *Rev. Sci. Instrum.* **89**, 015107 (2018).
43. Y. Tang, S. Bao, T. Kanai, W. Guo, Statistical properties of homogeneous and isotropic turbulence in He II measured via particle tracking velocimetry. *Phys. Rev. Fluids* **5**, 084602 (2020).
44. R. A. Sherlock, D. O. Edwards, Oscillating superleak second sound transducers. *Rev. Sci. Instrum.* **41**, 1603–1609 (1970).
45. R. T. Wang, C. E. Swanson, R. J. Donnelly, Anisotropy and drift of a vortex tangle in helium II. *Phys. Rev. B* **36**, 5240–5244 (1987).
46. M. S. Paoletti, M. E. Fisher, K. R. Sreenivasan, D. P. Lathrop, Velocity statistics distinguish quantum turbulence from classical turbulence. *Phys. Rev. Lett.* **101**, 154501 (2008).
47. M. S. Paoletti, R. B. Fiorito, K. R. Sreenivasan, D. P. Lathrop, Visualization of superfluid helium flow. *J. Phys. Soc. Jpn.* **77**, 111007 (2008).
48. A. A. Skoblin, D. V. Zlenko, S. V. Stovbun, Friction force limits the drift of microparticles along the quantum vortex in liquid helium. *J. Low Temp. Phys.* **200**, 91–101 (2020).
49. D. Ben-Avraham, S. Havlin, *Diffusion and Reactions in Fractals and Disordered Systems* (Cambridge University Press, Cambridge, UK, 2000).
50. R. J. Donnelly, C. F. Barenghi, The observed properties of liquid helium at the saturated vapor pressure. *J. Phys. Chem. Ref. Data* **27**, 1217–1274 (1998).
51. M. Tsubota, T. Araki, W. F. Vinen, Diffusion of an inhomogeneous vortex tangle. *Phys. B Condens. Matter* **329–333**, 224–225 (2003).
52. E. Rickinson, N. G. Parker, A. W. Baggaley, C. F. Barenghi, Inviscid diffusion of vorticity in low-temperature superfluid helium. *Phys. Rev. B* **99**, 224501 (2019).
53. Y. Sagi, M. Brook, I. Almog, N. Davidson, Observation of anomalous diffusion and fractional self-similarity in one dimension. *Phys. Rev. Lett.* **108**, 093002 (2012).
54. T. H. Solomon, E. R. Weeks, H. L. Swinney, Observation of anomalous diffusion and Lévy flights in a two-dimensional rotating flow. *Phys. Rev. Lett.* **71**, 3975 (1993).
55. T. H. Harris *et al.*, Generalized Lévy walks and the role of chemokines in migration of effector CD8+ T cells. *Nature* **486**, 545–548 (2012).
56. D. A. Raichlen *et al.*, Evidence of Lévy walk foraging patterns in human hunter-gatherers. *Proc. Natl. Acad. Sci. U.S.A.* **111**, 728–733 (2014).
57. R. Metzler, J. Klafter, The random walk's guide to anomalous diffusion: A fractional dynamics approach. *Phys. Rep.* **339**, 1–77 (2000).
58. J. P. Bouchaud, A. Georges, Anomalous diffusion in disordered media: Statistical mechanisms, models and physical applications. *Phys. Rep.* **195**, 127–293 (1990).
59. M. L. Mantia, L. Skrbek, Quantum, or classical turbulence? *Europhys. Lett.* **105**, 46002 (2014).
60. A. C. Davison, D. R. Cox, Some simple properties of sums of random variables having long-range dependence. *Proc. R. Soc. Lond. A* **424**, 255–262 (1989).
61. I. M. Mazzitelli, D. Lohse, Lagrangian statistics for fluid particles and bubbles in turbulence. *New J. Phys.* **6**, 203 (2004).
62. A. C. White, C. F. Barenghi, N. P. Proukakis, A. J. Youd, D. H. Wacks, Nonclassical velocity statistics in a turbulent atomic Bose-Einstein condensate. *Phys. Rev. Lett.* **104**, 075301 (2010).
63. A. Cidrim, A. C. White, A. J. Allen, V. S. Bagnato, C. F. Barenghi, Vinen turbulence via the decay of multicharged vortices in trapped atomic Bose-Einstein condensates. *Phys. Rev. A* **96**, 023617 (2017).
64. S. Yui, H. Kobayashi, M. Tsubota, W. Guo, Fully coupled dynamics of the two fluids in superfluid ^4He : Anomalous anisotropic velocity fluctuations in counterflow. *Phys. Rev. Lett.* **124**, 155301 (2020).
65. E. Fonda, K. R. Sreenivasan, D. P. Lathrop, Sub-micron solid air tracers for quantum vortices and liquid helium flows. *Rev. Sci. Instrum.* **87**, 025106 (2016).
66. I. F. Sbalzarini, P. Koumoutsakos, Feature point tracking and trajectory analysis for video imaging in cell biology. *J. Struct. Biol.* **151**, 182–195 (2005).